remote sensing

MDPI

Article

A River Basin over the Course of Time: Multi-Temporal Analyses of Land Surface Dynamics in the Yellow River Basin (China) Based on Medium Resolution Remote Sensing Data

Christian Wohlfart [1,*], Gaohuan Liu [2], Chong Huang [2,3] and Claudia Kuenzer [4]

1 Company for Remote Sensing and Environmental Research (SLU), Kohlsteiner Strasse 5, 81243 Munich, Germany
2 State Key Laboratory of Resources and Environmental Information System, Institute of Geographic Sciences and Natural Resources Research (IGSNRR), Chinese Academy of Sciences (CAS), 11A Da Tun Road, An Wai, Beijing 100101, China; liugh@lreis.ac.cn (G.L.); huangch@lreis.ac.cn (C.H.)
3 Jiangsu Center for Collaborative Innovation in Geographic Information Resource Development and Application, Nanjing, Jiangsu 210023, China
4 German Aerospace Center (DLR), German Remote Sensing Data Center (DFD), Münchner Strasse 20, 82234 Oberpfaffenhofen, Germany; claudia.kuenzer@dlr.de
* Correspondence: christian.wohlfanrt@remote-sensing-biodiversity.org; Tel.: +49-171-581-6950

Academic Editors: Magaly Koch and Prasad S. Thenkabail
Received: 8 December 2015; Accepted: 29 January 2016; Published: 26 February 2016

Abstract: The Yellow River Basin is one of China's most densely-populated, fastest growing and most dynamic regions, with abundant natural resources and intense agricultural production. Major land policies have recently resulted in remarkable landscape modifications throughout the basin. The availability of precise regional land cover change information is crucial to better understand the prevailing dynamics and underlying factors influencing the current processes in such a complex system and can additionally serve as a valuable component for modeling and decision making. Such comprehensive and detailed information is lacking for the Yellow River Basin so far. In this study, we derived land cover characteristics and dynamics from the complete last decade based on optical high-temporal MODIS Normalized Differenced Vegetation Index (NDVI) time series for the whole Yellow River Basin. After filtering and smoothing for noise reduction with the use of the adaptive Savitzky–Golay filter, the processed time series was used to derive a large variety of phenological and annual metrics. The final classifications for the basin (2003 and 2013) were based on a random forest classifier, trained by reference samples from very high-resolution imagery. The accuracy assessment for all 18 thematic classes, which was based on a 30% reference data split, yielded an overall accuracy of 87% and 84% for 2003 and 2013, respectively. Major land cover and land use changes during the last decade have occurred on the Loess Plateau, where land and conservation reforms triggered large-scale recovery of grassland and shrubland habitat that had been previously covered by agriculture or sparse vegetation. Agricultural encroachment and urban area expansion are other processes influencing the dynamics in the basin. The necessity for regionally-adapted land cover maps becomes obvious when our land cover products are compared to existing global products, where thematic accuracy remains low, particularly in a heterogeneous landscape, such as the Yellow River Basin. The basin-wide novel land cover and land use products of the Yellow River Basin hold a large potential for climate, hydrology and biodiversity modelers, as well as river basin and regional governmental authorities and will be shared upon request.

Keywords: land cover change; phenology; MODIS; random forest; time series analysis; Yellow River Basin

1. Introduction

River basins provide a variety of ecosystem services and goods and, thus, have led to the dawn of many ancient civilizations. Amongst others, they offer fertile soils, reliable water resources for drinking and irrigation and an easy way of transportation. For much of China, the Yellow River (Chinese: Huang He) is designated as the "cradle of civilization". With early settlements along the river banks, humans have shaped the river's landscape and hydro-physical characteristics for centuries. Today, the basin provides the livelihood for almost 190 million people and plays a vital role in China's continued economic development based on its abundant natural resources, including rare ores, coal, oil and gas, which make it one of China's most dynamic regions. Currently, the basin's provinces are attributed with annual GDP growth rates exceeding 10% [1]. As one of China's "breadbaskets", the region contains approximately 13 million ha of arable land, in which approximately 10 million tons of grain (in 2013) are produced, equivalent to nearly 20% of the domestic production [1–4]. Hence, the high demand for and intense use of the prevailing water and land resources have led to profound land use activities in the last few decades with adverse ecological, economic and social repercussions [5–8]. A river basin requires holistic management perspectives and reliable, consistent, multi-temporal information, and basin-wide land cover data are essential and can serve as baseline information for the acting stakeholders to support sustainable regional management applications and planning decisions.

Despite the urgent need to better understand the pressing land use dynamics in the Yellow River Basin, there is a surprising lack of comprehensive land cover information for the entire basin. In recent years, merely local land cover studies covering only small parts of the basin have been conducted, mainly focusing on the source region of the Yellow River [9,10], the highly erosive Loess Plateau in the middle reaches [11–13] or the fast-developing delta area [7,14]. To our knowledge, only two basin-wide products published by Li *et al.* [15] and Wang *et al.* [16] exist. The former study produced a thematic detailed mono-temporal land cover dataset for 1994, based on coarse resolution AVHRR (Advanced Very High Resolution Radiometer) imagery. The latter work is a multi-temporal change detection analysis between 1990 and 2000, which is derived from Landsat Thematic Mapper (TM) data. Both products are outdated and not applicable for analyzing the current and pressing dynamics in this region. Very often, the well-known global and continental datasets, such as the Global Land Cover 2000 product (GLC 2000) [17], GlobCover [18], MODIS land cover datasets [19] or the ESA Climate Change Initiative (CCI) Land Cover (CCI-LC) product [20], are often used to answer regional research questions, and they serve as a basis for many land use management plans and decisions. They have been derived from coarse to medium resolution Earth observation satellites, such as AVHRR, MODIS (Moderate-resolution Imaging Spectroradiometer) or the Medium Resolution Imaging Spectrometer (MERIS) instrument. Their ability for regionally-specific land cover analysis and land cover dynamics is hampered, as they were designed for global applications covering all vegetation and land cover types and, hence, are too generalized, particularly in heterogeneous landscapes, such as the Yellow River Basin [21–26].

Phenology-driven land cover classification schemes on different regional scales using high-temporal information have advanced, and the use of phenological variables as classification input features has proven to be a reliable classification input for large areas with heterogenic environmental conditions [14,27–29]. The MODIS sensor onboard the Terra and Aqua platforms can observe the entire Earth's surface with near daily global coverage. This multi-temporal datasets allow for the composition of high temporal time series that capture the signatures of the prevailing land cover entities, minimizing the influence of cloud coverage. Using this high temporal information on, e.g., vegetation indices, it is possible to effectively discriminate different land cover classes based on their intra-annual temporal signature [30].

In order to fill the existing research gap, this study addresses the urgent need for consistent and multi-temporal land cover products for the Yellow River Basin. We present a unique land cover analysis at a spatial resolution of 250 m for the years 2003 and 2013 and additionally evaluated the changes that occurred in this very dynamic region. The classification takes the advances of phenology-based metrics, derived from high temporal resolution MODIS NDVI (Normalized Differenced Vegetation Index) time series. This product is then compared to the previously-described global land cover products. For this purpose, 1380 MODIS scenes of five MODIS tiles for six years had to be processed. The generated consistent bi-temporal land cover data for the last decade are urgently required and needed to improve our understanding about the sweeping dynamics in the basin.

2. Study Area

The Yellow River Basin (32°N–42°N/96°E–119°E) is a major river watershed in northern China, and as the nation's second largest basin, drains a total area of approximately 750,000 km^2 [32]. Originating in the Qinghai-Tibet Plateau in western China, the river flows 5450 km, crossing nine Chinese provinces and emptying into the Bohai Sea, where the Yellow River Delta is formed (Figure 1). The climatic conditions are influenced by the continental monsoon circulation system. Mean annual precipitation throughout the basin equals around 500 mm, but is unevenly distributed across space and time [31]. The high altitude Qinghai-Tibet Plateau in the upper section receives around 300 mm per year, and average temperatures remain low (1–4 °C). Going further north, the area becomes more arid, with only 150 mm of rainfall annually. The lower and middle parts of the basin experience humid and sub-humid conditions with annual rainfall sums reaching up to 750 mm and temperatures ranging from 12–14 °C. A large part of the annual precipitation falls during the summer months (July and August), frequently in the form of heavy and intense summer storms [33]. These events are mainly responsible for the high soil erosion rates and the large quantities of sediment reaching the Yellow River and its tributaries [34]. Following the climatic gradient, the basin encompasses a wide range of different ecoregions [35]: the vast high-alpine southeast Tibet shrublands and meadows extend to the west, where nomadic pastoralism is still widespread. The Gobi Desert and the arid Ordos Plateau steppe, located in the north, are poorly suited for agricultural use due to infertile soils and scarce water resources. Further to the east lies the highly erosive Central Loess Plateau, with dissected and erosive loessal hills, and the flat Huang He (or North China) Plain, both of which are used intensively for agricultural production. The basin's landscape and river characteristics have been greatly affected by strong human activities, such as agriculture, particularly irrigation, the extraction of natural resources, industrialization and dam/infrastructure construction [6,16,36,37].

3. Material and Methods

The analytical framework of this study is based on high-temporal, medium-resolution Earth observation data. The data processing and reference data collection procedure is summarized in Figure 2. Seasonal and annual NDVI statistics based on MODIS time series served as input features for the random forest classifier. The two final thematic products were validated using a 30% reference data split. From the derived maps, we detected land cover changes and revealed local land surface dynamics in the last decade, which were examined quantitatively and qualitatively. By comparing local subregions, which are both complex and challenging, with high resolution Landsat imagery, we demonstrate that regional land cover products outperform the available global products.

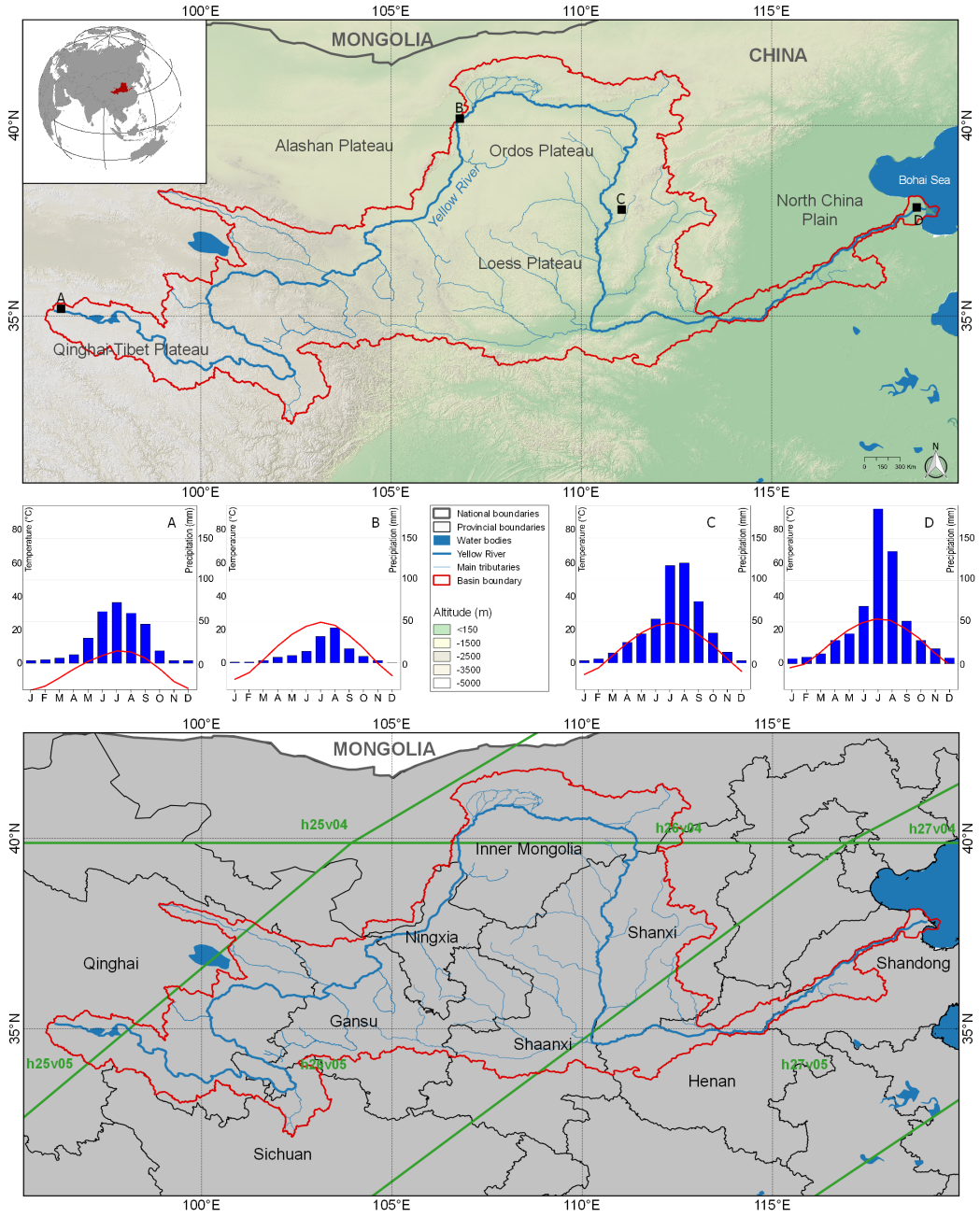

Figure 1. The top figure depicts the Yellow River Basin and its major geographical units. The selected diagrams show the different climatic patterns occurring in the basin. The underlying climate data were derived from Hijmans *et al.* [31]. The bottom figure displays the provinces embedded in the basin and the MODIS footprints covering the entire study area.

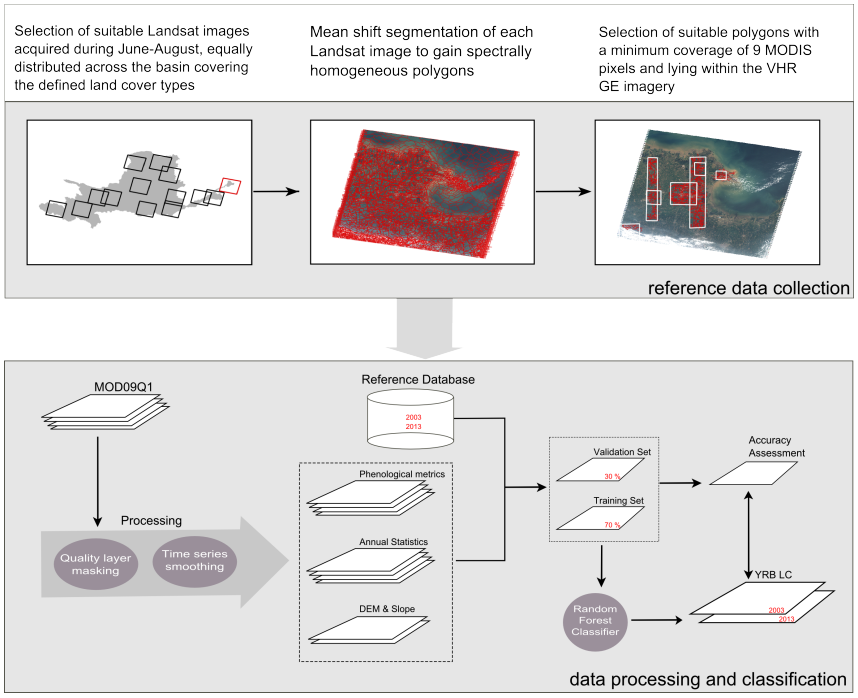

Figure 2. Flowchart depicting the reference data collection steps (**top**) and the processing and classification procedure (**bottom**) to derive the Yellow River Basin land cover product (YRB LC).

3.1. MODIS Data and Processing Steps

The MODIS surface reflectance product MOD09Q1 served as the backbone of the study and was acquired for two time spans, from January 2002–December 2004 and from January 2012–December 2014 (Figure 2 (bottom)). Although we only focused on 2003 and 2013, it was necessary to process three consecutive years for each time step, in order to guarantee the proper calculation of the start/end of the season of the central year. In order to ensure full data coverage of the basin, we selected a total of five MODIS tiles (h25v04, h25v05, h26v04, h26v05, h27v05) (Figure 1). The MOD09Q1 8-day composite contains three data layers at a 250-m spatial resolution: MODIS Band 1 (red channel, 620–670 nm), Band 2 (near-infrared channel, 841–876 nm) and the MODIS Quality Assurance (QA) layer [38]. A total of 1380 MODIS scenes were acquired and processed. For data download and initial processing steps, we used the statistical programming environment R [39] and the package *MODIS*, which incorporates automatic download and processing functions, such as reprojection, mosaicking and subsetting [40]. For each scene, the native sinusoidal projection was converted to the geographical latitude/longitude projection (WGS84 datum), keeping the 250-m spatial resolution. MODIS imagery is inherently influenced by atmospheric and geometric interferences and noise; thus, we applied a quality assessment at the pixel level for each band and used only the "highest" quality pixels provided by the QA layer. Low quality pixels were masked out. With the cleaned bands, the Normalized Difference Vegetation Index (NDVI), which was based on surface reflectance Bands 1 and 2, was calculated for the full 13-year time series with 46 time steps each year. The interpolation of the gaps and additional noise reduction was achieved by applying adaptive Savitzky–Golay (SG) filtering using TIMESAT software, which was specifically designed for analyzing time series of satellite imagery [41]. The SG filter is a moving window filter that performs a polynomial least-squares fit of a certain degree to all points in the window and replaces the central point with the value of the polynomial [42]. In TIMESAT, the SG algorithm is implemented in a newly-adapted form. Sometimes, the globally-defined window size does not account for rapid increases or decreases in the NDVI trajectory. In these cases, it is necessary to locally decrease the

window with a smaller one [41]. This filter type has the ability to follow rapid changes within the time series. Within the Yellow River Basin, intensified agriculture with a two-season cropping cycle is widespread, so we used a rather small window size of five as tested by Leinenkugel *et al.* [29] to capture the fast changing phenology within a year.

3.2. Classification Features

The advantages of using phenological and annual metrics derived from high temporal and medium spatial resolution remote sensing imagery as predictors for land cover classification have been demonstrated in many broad-scale land cover studies, e.g., [30,43]. Every land cover class consists of its individual temporal NDVI profile and is represented in the computed phenological metrics for land cover discrimination, as shown in Figure 3. From the previously-filtered and smoothed MODIS NDVI time series, we computed various seasonal phenology metrics, characterizing the growing and biological cycle throughout the year. We derived eleven metrics as defined and described by Jönsson and Eklundth [41] for 2003 and 2013. Furthermore, several annual statistics were extracted for the NDVI and both spectral bands (RED and NIR), *i.e.*, the median, standard deviation or different percentiles (10, 25, 75, 90 percentiles) and their differences (75th–25th percentile, 90th–10th percentile). Additionally, we added a digital elevation model (DEM) and slope as additional predictors. In total, this results in 37 input features for the classifier (see Table 1).

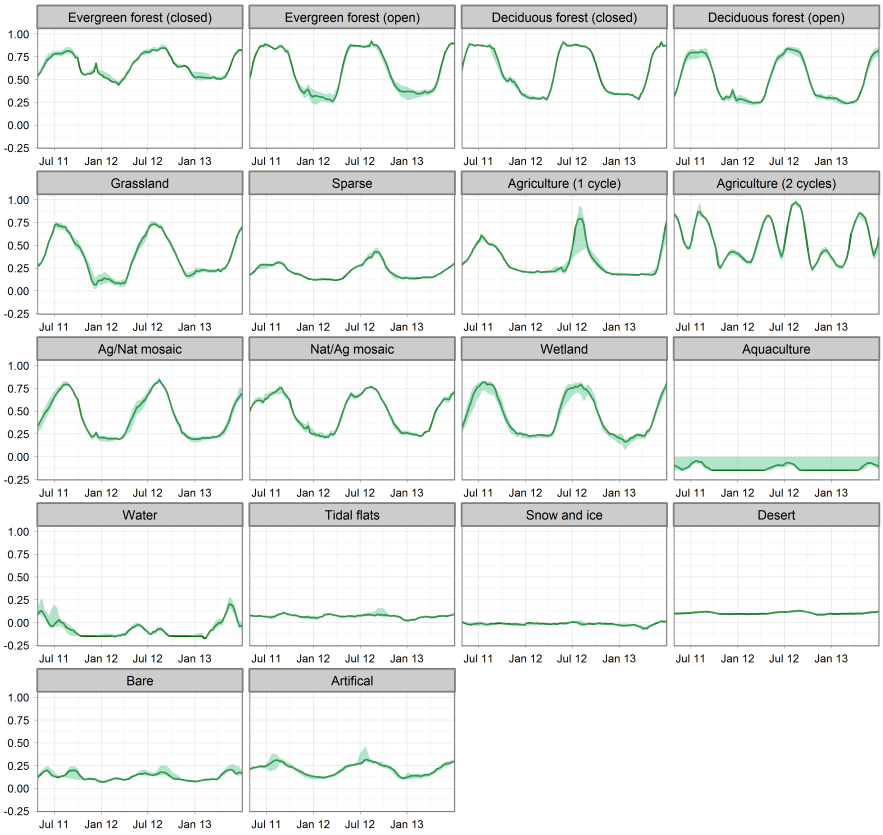

Figure 3. Average temporal NDVI trajectories, derived from 8-day MOD09Q1 data, of all land cover types occurring in the Yellow River Basin (green line) for 3 consecutive years (2012–2014); the light-green shaded area represents the 10th and 90th percentile, respectively.

Table 1. Phenological and annual metrics and their description. The latter were calculated for the Vegetation Index and both spectral channels (RED, NIR).

	Metrics	Description
Seasonal metrics	Start of season	Time for which the left edge has increased to 40% of the seasonal amplitude measured from the left minimum level
	End of the season	Time for which the right edge has decreased to 40% of the seasonal amplitude measured from the right minimum level
	Length of the season	Time from the start to the end of the season
	Base level	Average of the left and right minimum values
	Middle of the season	Mean value of the times for which the left edge has increased to the 80% level and the right edge has decreased to the 80% level
	Peak value	Largest value between the start and end of the season
	Seasonal amplitude	Difference between the peak value and the base level
	Rate of increase at the beginning of the season	Ratio of the difference between the 20% and 80% levels and the corresponding time difference
	Rate of decrease at the end of the season	Ratio of the difference between the right 20% and 80% levels and the corresponding time difference
	Large seasonal integral	Integral of all values between the start and the end of the season
	Small seasonal integral	Integral of all values from the start to the end of the season minus the base level
Annual metrics	Median	Median value derived from annual multi-temporal statistics
	Standard deviation	Standard deviation from annual multi-temporal statistics
	10th percentile	10th percentile value from annual multi-temporal statistics
	25th percentile	25th percentile value from annual multi-temporal statistics
	75th percentile	75th percentile value from annual multi-temporal statistics
	90th percentile	90the percentile value from annual multi-temporal statistics
	Diff 90th–10th percentile	Difference between 90th and 10thpercentile
	Diff 75th–25th percentile	Difference between 75 and 25 percentile

3.3. Reference Data Collection

For remote sensing-based land cover analysis, it is important to rely on a high quality reference database for training and testing. A faulty and inappropriate sampling scheme can introduce much error, influencing the reliability of the final classification. In September 2013, a two-week field campaign was conducted in the Yellow River Basin. In the field, we collected suitable reference samples of homogeneous areas. However, the collection of a valid amount of representative samples to characterize the prevailing land cover for the entire study area was not possible in an *in situ* field campaign throughout a region covering around 750,000 km^2. Therefore, we additionally used high-resolution data from Landsat TM/OLI sensors and complementary very high-resolution (VHR) imagery provided in virtual globe software, such as Google Earth and Mapworld, to collect a comprehensive reference dataset for training and validation, as is often applied in large-scale and medium-resolution remote sensing studies [26,44,45]. The VHR imagery available in our study region stems mainly from Digital Globe's Quickbird and GeoEye's IKONOS satellites.

First, we defined adequate thematic land cover classes for the Yellow River Basin (see Table 2) by interpreting various sources and databases, including existing region-specific land cover descriptions, expert knowledge and VHR imagery in combination with geo-referenced photographs. The following sampling steps were carried out independently for 2003 and 2013 (Figure 2, top chart). First, we acquired suitable, fairly cloud-free and temporally-consistent Landsat scenes between June and August ensuring fully-developed vegetation. The collected Landsat tiles are equally distributed across the study area to capture all land cover entities (Figure 4). For each year, we determined 14 Landsat images. The next step involved retrieving spectrally- and texturally-homogeneous objects. This has been achieved with the Orfeo ToolBox (OTB), a library for processing remote sensing imagery. Within the OTB, a segmentation application is included, which allows for the multispectral segmentation of raster images. We included all spectral Landsat bands, as well as the NDVI in the segmentation process and applied the implemented mean-shift segmentation algorithm, grouping and generating objects with similar spectral and textural properties. As a minimum sampling unit, we defined objects covering at least an area of nine MODIS pixel, as suggested by Congalton and Greene [46]. As a clear visual interpretation of the prevailing land cover is only possible from high quality and high resolution data, we selected polygon objects embedded in available VHR Google Earth data. Nonetheless, the marginal areas of each object might still be influenced by mixed pixels. The negative buffering of one MODIS pixel removes the potential transitional pixels to further guarantee the homogeneity of the reference objects.

Table 2. Name and description of all defined land cover classes in the Yellow River Basin.

ID	Class name	Description
1	Evergreen needle-leaved forests (closed)	Forest with predominant evergreen needle-leaved tree species, covering at least 65% and height exceeding 2 m
2	Evergreen needle-leaved shrub and woodland (open)	Evergreen needle-leaved forests covering 15%–40% and mixed with grassland and/or shrub entities.
3	Deciduous broadleaved forests (closed)	Forest with predominant broadleaved deciduous tree species, covering at least 65% and height exceeding 2 m
4	Deciduous broadleaved shrub and woodland (open)	Deciduous broadleaved forests covering 15%–40% and mixed with grassland and/or shrub entities
5	Grassland	Herbaceous vegetation layer with less than 10% woodland and shrub coverage
6	Sparse vegetation	Sparse shrub and herbaceous vegetation entities covering 5%–15%
7	One season cropland	Agricultural areas with one harvest per year
8	Two season cropland	Agricultural areas with two harvests per year
9	Natural vegetation/agriculture mosaics	Predominant natural vegetation entities (grassland, shrub, woodland), accompanied with cropland
10	Agriculture/natural vegetation mosaics	Predominant cropland, accompanied with natural vegetation entities
11	Aquaculture	Water ponds used for aquaculture production, mainly for fish, crustaceans and turtles, usually surrounded and intersected with grassland
12	Wetlands	Areas saturated with salt or fresh water with a permanent mosaic of water and herbs or woodland
13	Water bodies	Areas covered with either fresh or salt water
14	Tidal flats	Coastal wetlands exposed to tidal amplitude consisting of unconsolidated sediments
15	Snow and ice	Areas permanently covered by snow or ice
16	Deserts (sandy)	Barren area covered by sand dunes
17	Bare areas	Barren land with natural vegetation less than 5%
18	Artificial areas	Built up areas and associated areas

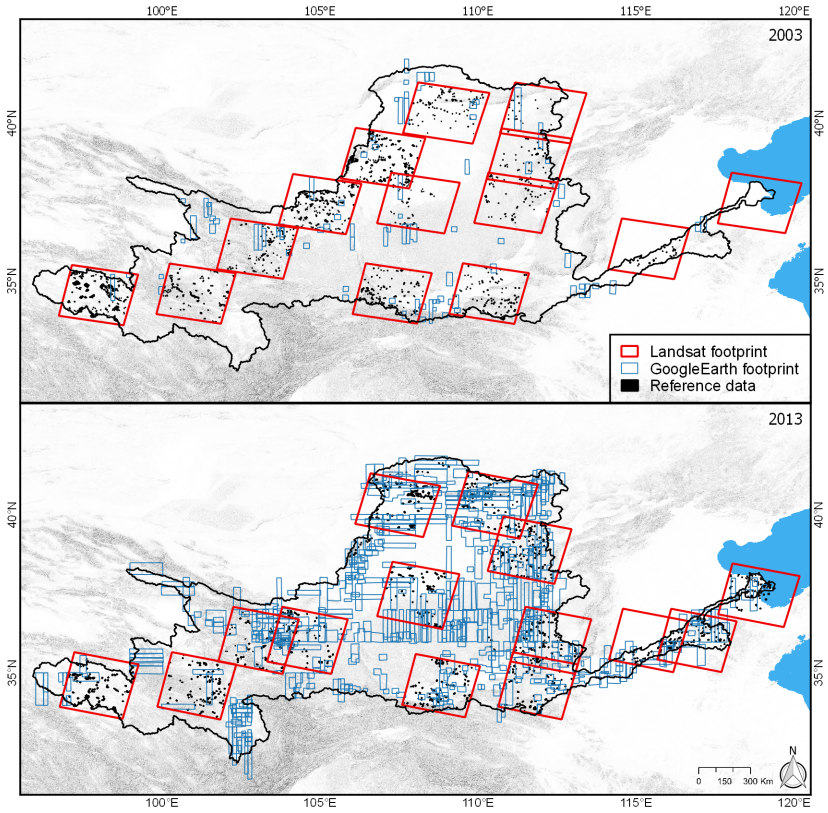

Sensor	Acquisition date	Path/Row	Center location
Landsat 5 TM	2003-08-07	121/34	37.5°N/119.0°E
Landsat 5 TM	2003-06-18	123/35	36.1°N/115.1°E
Landsat 5 TM	2003-07-09	126/32	40.0°N/112.1°E
Landsat 5 TM	2003-06-07	126/33	38.9°N/111.5°E
Landsat 5 TM	2003-06-23	126/34	37.5°N/111.1°E
Landsat 5 TM	2003-06-23	126/36	34.5°N/110.3°E
Landsat 5 TM	2003-06-05	126/36	40.3°N/108.9°E
Landsat 5 TM	2003-06-05	128/34	37.5°N/108.1°E
Landsat 5 TM	2003-06-05	128/36	34.6°N/107.2°E
Landsat 5 TM	2003-06-12	129/33	38.9°N/106.9°E
Landsat 5 TM	2003-06-19	130/34	37.4°N/104.9°E
Landsat 5 TM	2003-07-17	134/36	34.5°N/97.9°E

Sensor	Acquisition date	Path/Row	Center location
Landsat 8 OLI	2013-06-30	121/34	37.5°N/119.0°E
Landsat 8 OLI	2013-06-21	122/35	36.0°N/116.9°E
Landsat 8 OLI	2013-06-13	123/35	36.0°N/115.4°E
Landsat 8 OLI	2013-08-30	125/35	36.1°N/112.3°E
Landsat 8 OLI	2013-08-05	126/33	34.6°N/111.9°E
Landsat 8 OLI	2013-08-12	127/32	38.9°N/111.5°E
Landsat 8 OLI	2013-06-25	127/36	34.5°N/108.8°E
Landsat 8 OLI	2013-08-03	128/34	37.5°N/108.0°E
Landsat 8 OLI	2013-08-01	130/35	40.3°N/107.2°E
Landsat 8 OLI	2013-08-08	131/35	36.0°N/102.9°E
Landsat 8 OLI	2013-08-15	132/36	34.6°N/101.1°E
Landsat 8 OLI	2013-08-13	134/36	34.5°N/97.9°E

Figure 4. Location and extent of Landsat (red) and very high-resolution (VHR) imagery (blue) footprints for 2003 (**top**) and 2013 (**bottom**). The table below shows meta-information for each respective Landsat image.

To ensure an unbiased distribution of objects across the study area, we randomly generated 2500 points and selected the corresponding polygon. Simple random sampling is the least biased sampling technique, because all parts of the study area have an equal chance of being selected. For each land cover class, we decided to select at least 100 samples, as suggested by several authors [46–48], to get a representative and statistically-valid representation of the complex landscape. A larger sampling size has been gained for dominant land cover classes and those classes with inherent variability and complexity [49]. Finally, we assigned the class-specific ID code to each polygon by visual interpretation. The drawback of simple random sampling is, however, that small and rarely-occurring areas may be under-represented, because they do not ensure a uniform distribution of points across the landscape. This problem has also appeared in our sampling strategy. We therefore manually sampled underrepresented land cover classes until at least 100 samples had been taken. For all collected samples, we kept a minimum sampling distance of at least 30 MODIS pixels to avoid spatial autocorrelation effects and removed all objects not fulfilling this criterion. The final reference dataset for training and testing contained a total of 2340 objects for 2003 and 2232 for 2013. The distribution of each reference dataset can be obtained in Figure 4.

3.4. Classification Approach, Post-Classification and Accuracy Assessment

Various classification models for land cover applications have been used, such as the generalized linear model (GLM), support vector machine (SVM) or decision tree learning, among others. Decision tree-based classifiers, such as random forests (RF), have been successfully and extensively applied to land cover studies and tend to yield higher accuracies than other conventional classifiers, including maximum likelihood and standard trees [50–52]. Aside from the high performance, RF is robust to noise and overfitting, and the algorithm is comparably quicker than methods based on boosting [53]. Further, the handling of the classifier is user-friendly, as the model can be run without much tuning of the parameters. In this study, the entire RF classification was carried out using R and the package *randomForest*implementing Breiman's random forest algorithm [54]. RF algorithms are used to construct multiple decision trees, which are built independently, using a bootstrap sample of the dataset [53]. RF searches for a random sample of the predictors and chooses the best split amongst the predictors. The final classification is based on the majority vote of the ensemble. Here, we built up an RF model with 300 individual trees, as prior testing showed a convergence of the mean squared error (MSE) at that value. For further model tuning and building, we applied the R package *caret* developed by Kuhn *et al.* [55], resulting in a final *mtry*value of 15 for both years. This value describes how many variables are sampled at each split. The RF classifier ran independently for 2003 and 2013. *Caret* integrates a measure of predictor importance to see which variable were the most informative in making distinctions between the land cover classes. This measure is scaled from 0–100. To generate an unbiased and stable selection of important and non-important variables prior to fitting the RF model, the Boruta algorithm was applied [56]. This algorithm tests if variables are expected to be less important than random samples. No variable was deemed to be non-important.

The thematic accuracy of the two final land cover products was assessed by splitting the comprehensive reference dataset polygon-wise into a 30% proportion set. The remaining 70% served as the training samples. We chose the 70/30% split option as it performs best using RF algorithms, as demonstrated by Adelabu *et al.* [57]. The use of confusion matrices is a clear way to present the accuracy, which contains class-specific user's, producer's and overall accuracy [46,58].

Many land cover classes that we defined show similar spectral and temporal responses, making their exact classification ambiguous. Therefore, several logical post-classification rules using ancillary data were defined to improve the classification accuracy (Figure 5). For instance, mountain shadows are often misclassified as water. To correct for this issue, the slope calculated from a DEM was superimposed, and all water bodies with an inclination >1° were reclassified to the bare class, as lentic water is not present on slopes. The spectral differentiation between barren land on steep slopes and artificial surfaces was revealed to be a challenge. The auxiliary Nighttime Lights Time

Series (Version 4) derived from the DMSP Operational Linescan System (OLS) instruments served as an indication for urban and built-up structures [59]. As suggested by Small *et al.* [60], we applied a threshold of >86% to detect lighted urban areas. Double-cropping cycles of wheat-maize or wheat-soybean are very common in the Yellow River Basin, particularly in the North China Plain, where favorable environmental conditions are present [61]. As additional output, TIMESAT delivers a mask with information about seasonal cycles, and we reclassified the agricultural class accordingly.

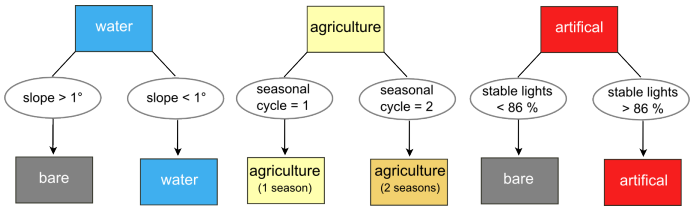

Figure 5. Post-classification decision rules for the Yellow River Basin land cover classification.

4. Results

The result are presented in three main parts; for the first of which, we highlight the novel bi-temporal land cover products for the Yellow River Basin for 2003 and 2013 and describe the current land cover features, focusing specifically on each ecoregion. Additionally, we reveal land dynamics throughout the basin that have occurred in the last decade. Local hotspot regions of change are shown, focusing on different land cover types. Next, we compare our derived product to existing global and national land cover datasets by selecting local case study sites representing some of the basin's complex land cover structure.

4.1. Current Land Cover Characteristics and Dynamics in the Yellow River Basin

The classification outcome of the Yellow River Basin land cover products (YRB LC 2003 and 2013) is presented in Figure 6, with an overall accuracy of 87% and 84% for 2003 and 2013, respectively. We computed class-specific user's and producer's accuracy, which are summarized in the confusion matrices in Table 3. The generated products depict a detailed extent and distribution of the current land cover status and dynamics, not presented in previous land cover studies thus far. We adapted and defined the classes specifically for the Yellow River Basin, including classes of natural vegetation (terrestrial and aquatic), cultivated classes, mosaic classes, and non-vegetated, artificial classes, resulting in a total of 18 land cover classes. The land cover proportions and their changes between 2003 and 2013 for the basin's four major geographical units, the Qinghai-Tibet Plateau, Ordos Plateau, Loess Plateau and North China Plain, including the delta region (Figure 1, top), can be obtained from Figure 7. The land cover proportions for the entire basin for 2003 and 2013 are summarized in Table 4. The land cover forms show significant variation across the basin, as can be seen in Figure 7. The vast elevated Qinghai-Tibet Plateau is dominated by alpine grasslands covering around 65% in 2013. Vegetation form and land cover proportions change significantly in the Ordos Plateau steppe, where sparsely-vegetated and barren areas are predominant. Agricultural production is only possible along the river banks. The Loess Plateau, natively covered by extensive deciduous forest structures, is presently a major area for agriculture cultivation. The degree and extent of cultivation processes throughout the basin climaxes in the fertile and vast North China Plain, where a greater part of the land surface is dominated by agriculture.

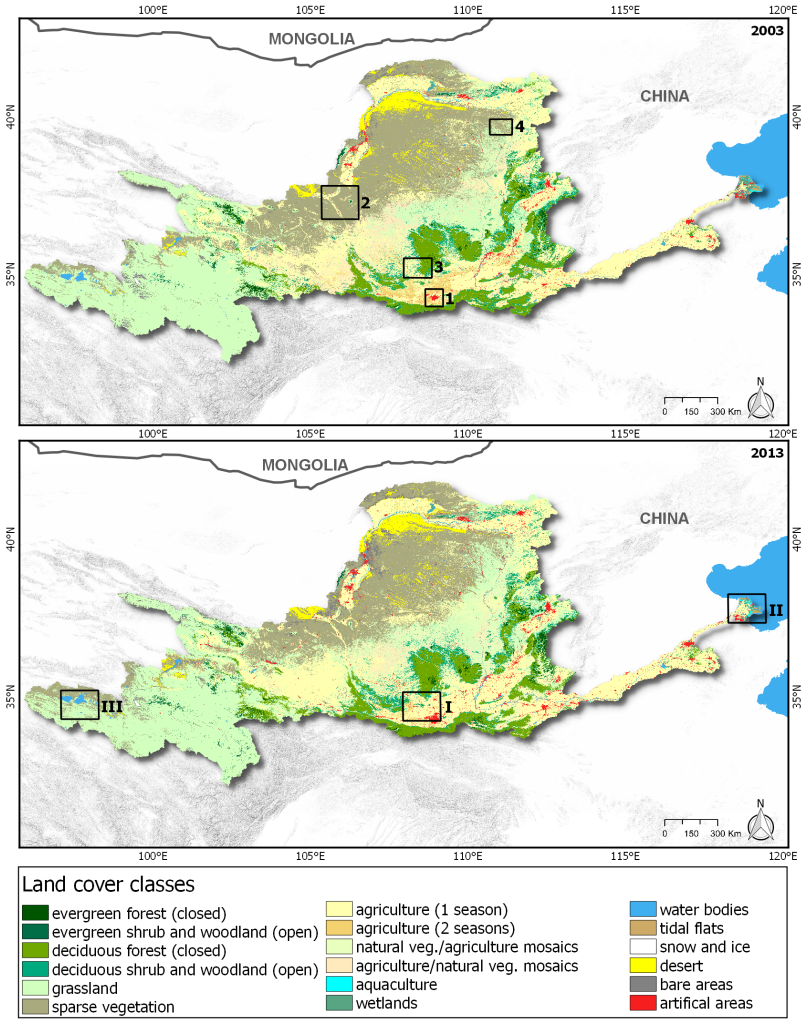

Figure 6. Land cover classification products for the Yellow River Basin (YRB LC) for 2003 (**top**) and 2013 (**bottom**). Framed areas in the top panel mark the regions with significant land cover changes shown in Figure 9. The subsets in the bottom panel were used for comparing our Yellow River classification product with existing global products depicted explicitly in Figure 10.

Figure 7. Land cover proportions for each ecoregion and year (2003, **left**; 2013, **right**). The color code of the different land cover types conforms to the colors introduced in Figure 6. The coverage of each ecoregion can be seen in Figure 1.

Table 3. Confusion matrix showing user's and producer's accuracy for each class and overall accuracy in percent for 2003 (**top**) and 2013 (**bottom**).

		Reference																
	2003	**1**	**2**	**3**	**4**	**5**	**6**	**7**	**9**	**10**	**11**	**12**	**13**	**14**	**15**	**16**	**17**	**18**	**UA (%)**
Classification	1	89.15	9.52	0	1.06	0.26	0	0	0	0	0	0	0	0	0	0	0	0	89.15
	2	14.18	82.53	0.46	2.30	0.23	0	0	0	0	0	0	0	0	0	0	0	0	82.53
	3	3.61	1.45	92.29	1.69	1.3	0	0	0	0	0	0	0	0	0	0	0	0	92.29
	4	0.22	3.23	0	78.06	3.36	0	1.29	5.26	3.2	0	0	0	0	0	0	0	0	78.06
	5	0	0.60	0	7.01	69.14	0	0	7.21	5.01	0	5.21	0.20	5.01	0	0	0.60	0	69.14
	6	0	0.72	0	0	1.67	83.73	0.48	0	0	0	0	0	0	0	0	3.59	6.46	83.73
	7	0	0	0	0	0.45	0	82.21	5.63	10.14	0.23	1.13	0	0	0	0	0.23	0	82.21
	9	0	0	0	7.6	7.04	0.29	4.40	79.77	0.3	0	0	0	0	0	0	0	0.29	79.77
	10	0	0	0	1.13	0.91	0.45	8.14	1.58	87.10	0	0	0	0	0	0	0	0	87.10
	11	0	2.5	0	0	0	0	0	0	0	94.00	0	5.99	0	0	0	0	0	94.00
	12	0	0	0.43	0	0	0	1.10	0	0	0.82	97.3	0.55	0	0	0	0	0	97.30
	13	0	0	0	0	0.23	0	0	0	0	11.9	0.35	82.00	0	5.69	0	0	0	82.00
	14	0	0	0	0	0	0	0	0	0	0	3.5	0.23	96.26	0	5.69	0	0	96.26
	15	0	0	0	0	0	0	0	0	0	0	0	1.05	0	98.94	0	0	0	98.94
	16	0	0	0	0	0	1.12	0	0	0	0	0	0	0	0	98.92	13.09	0	98.92
	17	0	0	0	0	0.23	5.25	0	0	0	0	0	0	2.94	3.15	0	77.73	5.46	77.73
	18	0	0	0	0	1.21	5.84	0	0	0	0.25	0	0.73	3.65	0	3.15	0.49	87.59	87.59
	PA (%)	81.01	84.47	90.97	80.67	84.14	85.99	85.28	76.40	81.57	87.31	88.33	90.68	88.41	92.16	90.23	82.96	86.96	86.83

		Reference																
	2013	**1**	**2**	**3**	**4**	**5**	**6**	**7**	**9**	**10**	**11**	**12**	**13**	**14**	**15**	**16**	**17**	**18**	**UA (%)**
Classification	1	94.04	4.70	1.25	0	0	0	0	0	0	0	0	0	0	0	0	0	0	94.04
	2	5.91	89.83	0.47	0.95	2.36	0	0.24	0.24	0	0	0	0	0	0	0	0	0	89.83
	3	0.48	1.45	91.04	5.57	0.48	0	0	0	0.24	0	0.73	0	0	0	0	0	0	91.04
	4	1.66	13.39	6.98	65.96	2.99	0	0	11.87	1.06	0	0	0	0	0	0	0	0	65.97
	5	0	0.92	0.23	10.30	64.32	0.23	5.72	5.95	9.34	4.15	0	0.23	0	0	0	0.69	0.12	64.32
	6	0	0	0	0	0.97	71.07	1.94	0.39	0.19	0	4.47	0.19	0	0	1.75	12.62	6.21	71.07
	7	0	0	0	0.25	1.27	0	90.93	1.01	1.01	3.54	0.76	0.51	0	0.19	0	0	1.10	90.93
	9	0	0.44	0.22	5.01	8.71	0.65	1.09	76.25	6.97	0	0	0	0	0	0	0.22	0.44	76.25
	10	0	0	0	0.84	2.51	0.42	9.41	12.55	74.27	0	0	0	0	0	0	0	0	74.27
	11	0	0	0	0	0	0	0.48	0	0	92.36	0	5.97	1.19	0	0	0	0	92.36
	12	0	0	0.53	0.26	0	0	2.65	0.26	0	2.38	92.59	0.26	0.53	0	0	0	0.53	92.59
	13	0	0	0	0	0	0	0	0	0	12.27	0	87.50	0	0	0	0	0	87.50
	14	0	0	0	0	0	0	0	0	0	0.27	0	0	98.94	0	0	0	0	98.94
	15	0	0	0	0	0.25	0	0.23	0	0	1	0	0	0	98.15	0	0	0	98.15
	16	0	0	0	0	0	1.26	0	0	0	0	0	0	0	0	97.47	1.27	0	97.47
	17	0	0	0	0	0	8.88	0.51	0	0	0	0.91	1.27	2.54	2.1	2.5	76.14	9.4	76.14
	18	0	0	0	0	0	3.05	.910	0	0	0.30	0.80	2.13	2.13	0	0	1.22	91.50	91.50
	PA (%)	90.36	84.07	92.38	71.23	78.68	86.73	77.48	71.57	80.32	79.30	90.91	90.17	90.17	98.30	95.54	79.37	81.08	84.31

Table 4. Total area in km^2 and in the percentage of the total area for each land cover class and year.

	2003		**2013**	
Class ID	**Area (km^2)**	**Area (%)**	**Area (km^2)**	**Area (%)**
1	32,663	0.88	33,992	0.92
2	30,425	0.82	25,828	0.70
3	261,110	7.03	271.269	7.31
4	127,876	3.44	135,607	3.65
5	1,049,087	28.26	1,053,858	28.39
6	759,812	20.47	723.970	19.50
7	895,934	23.93	902,009	25.37
8	63,480	1.69	15,582	0.42
9	90,534	2.44	199,671	5.38
10	153,710	4.14	46,135	1.24
11	5123	0.14	7269	0,20
12	8992	0.24	7752	0.21
13	23,797	0.64	22,427	0.60
14	2003	0.05	2782	0.07
15	1319	0.04	1359	0.04
16	100,075	2.70	92,849	2.50
17	44,907	1.21	44,004	1.19
18	63,676	1.72	87,332	2.35

4.1.1. The Qinghai-Tibet Plateau

The Qinghai-Tibet Plateau is the world's highest and largest grassland plateau and feeds many of Asia's most important rivers. With altitudes exceeding 4500 m, the plateau is characterized by harsh environmental conditions with low temperatures and little precipitation. The landscape is dominated by relatively homogeneous alpine grassland tundra accompanied with areas of spare vegetation and bare areas. The homogeneous grassland systems achieved in this region higher user's (89%) and producer's (91%) accuracies compared to, e.g., the Loess Plateau, where accuracies are

considerably lower. Around 65% of the plateau is covered with grassland, as can be seen in Figure 7. This figure has not changed in the last 10 years. A marginal increase of sparse vegetation cover at the costs of grassland is detected in the vicinity of the two freshwater lakes, the Gyaring and Nyoring lakes. At the eastern foothills and in river valleys with milder climatic conditions, open and closed needle-leaved forest patches can be found. Glacier remnants are present in the ranges of the A'nyê Magên Mountains. The harsh environmental conditions make crop cultivation rather difficult. Only in low altitude valleys with milder climates are farmers able to grow wheat and vegetables in small-scale and subsistence agriculture.

4.1.2. The Ordos Plateau Steppe

Northward, there lies the extensive desert and steppe-like Ordos Plateau. Because of the arid conditions, dry-adapted and resistant xeric shrubs and grassland vegetation become more dominant, covering the surface very sparsely. The lack of precipitation in conjunction with non-nutritious soils inhibit productive cultivation of land for agriculture. Exceptions are small scattered oases throughout the steppe, along the banks of the Yellow River and large-scale irrigation districts, where sufficient water is available to grow crops. Irrigation farming is practiced in two major irrigation districts: the Qingtongxia district in the west and the Hetao district to the north. The main cultivated crops in this region are corn and wheat [62]. The Ordos region also comprises two large sandy deserts covering an approximate area of 6%: the Kubugi Desert in the north and the Maowusu Desert further south, with sparse vegetation along the sandy dunes. Since 2003, the proportions of sparse vegetation have declined by approximately 17%, being replaced mainly for agricultural purposes and for areas of mixed grassland/cropland mosaics. Further, urban and built-up areas have significantly expanded, particularly along the river banks.

4.1.3. The Loess Plateau

In contrast to the Ordos Plateau, the Loess Plateau is attributed with fertile, but highly erosive soils, allowing for cultivation. Once covered by dense vegetation, dominated by temperate open and closed deciduous (mainly oak, birch) and in higher altitudes by evergreen forests (spruce, mountain-ash), a long history of deforestation and over-grazing has turned the Loess Plateau into a degraded region with high erosion rates [63]. Many Yellow River tributaries originate on the central Loess plateau and cut the hilly area into numerous narrow ridges and mounds, making the surface rugged and uneven. At the eastern margins of the basin, the Loess Plateau consists of still extensive mixed deciduous forests in the Lu Liang Mountains, which gradually changes south-eastward to low steppe vegetation. In 2013, forest and woodland structures (open and closed) share an area of around 15,000 km^2, equal to 30% of the Loess Plateau, and this has not changed significantly during the last decade. The central part is characterized by small-scale mosaics of cropland and natural vegetation and areas of sparse vegetation, particularly on sloping areas. Until 2013, the proportion of natural vegetation and mixed cropland patches has significantly increased, while sparsely-vegetated areas have dwindled. Particularly, the mosaic class, having agriculture as the major land form, was transformed to the class "natural/agriculture vegetation mosaics", with a predominant share of natural vegetation. Many land policies and conservation programs have been launched, implementing terracing and greening the slopes to mitigate and stop the massive silt loads entering the Yellow River. The booming economy, mainly based on coal and chemical production, has led to an increase in urban and built-up areas in this region. Today, 50 million people populate the entire Loess Plateau.

4.1.4. The North China Plain and Delta

Further south, the North China Plain commences with the wide and densely-populated valley of the Wei River, the largest tributary of the Yellow River, which embodies one of the oldest irrigation districts in China. Through canals, the water is distributed across the valley, supplying major cities,

which considerably sprawled during the last decade by 24%; a similar figure was suggested by [1] (Figures 6 and 7 and Table 4). The Qinling Mountain Range delimits the Yellow River Basin to the south. The dominant vegetation forms are temperate deciduous forest ecosystems. Following the Yellow River eastwards towards the Bohai Sea, the vast alluvial region is dominated by a high level of intensified agricultural production, producing wheat, corn, sorghum and cotton, covering around 66%. Between 2003 and 2013, the cultivated area increased by 5%, which is by far not the order of magnitude of the crop output, which increased by 22% [1]. As suggested by Li *et al.* [61], cropping intensity is achieved by switching from single- to double-cropping cycles. This is obviously not the case in the Yellow River Basin, where cropping cycles decreased considerably, which is in accordance with data provided by the National Bureau of Statistics of China, indicating a reduction of two seasonal crops. Henan and Shandong are the most populous provinces located in the Yellow River Basin.

The Yellow River Delta is considered one of China's key regions in terms of economic development and has intensely evolved during the last few decades. The fertile soils make intensified agricultural crop cultivation possible. Furthermore, the high abundance of oil and gas resources triggered a rapid industrialization and urbanization in this region. Along the coastline, many ponds emerged for aquaculture practices and are still expanding (increase by 14%). All of this has harnessed the ecologically-sensitive delta area, one of only a few remnants of wetland ecosystems that remain, which are vitally important to local and even global avian biodiversity. To protect this sensitive area, the Yellow River Delta Nature Reserve was founded and consistently expanded during the last few years.

4.2. Variable Importance

The importance measures for 2003 and 2013 of all 37 MODIS predictors for land cover distinction in the Yellow River Basin are depicted in Figure 8, ordered from most to least important. Both years show similar patterns. The seasonal and small percentiles (10% and 25%) for both spectral bands and NDVI rank amongst the most relevant metrics in delineating the land cover for the basin. Base level, amplitude, peak value and the NDVI integral are found to be the most important seasonal metrics, while left derivative, middle season and the large integral remain least important. Likewise, higher percentiles (50% and 75%), as well as slope and altitude play a minor role in land cover delineation.

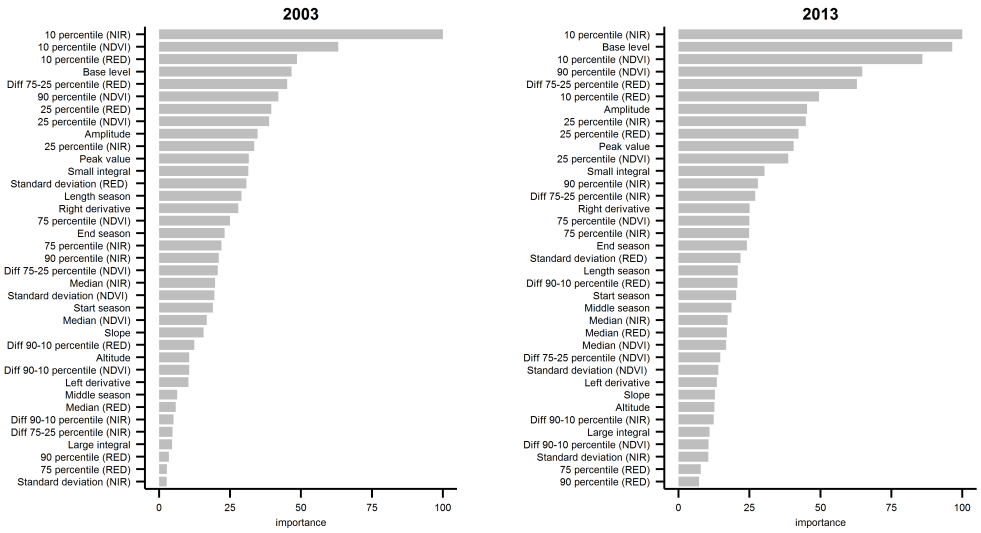

Figure 8. Importance of each predictor variable used in the random forest classifiers for 2003 (**left panel**) and 2013 (**right panel**), scaled from 0–100.

4.3. Local Dynamic Hotspot Regions in the Basin

The Yellow River Basin has undergone tremendous land cover dynamics during the last decade, triggered by recent socio-economic developments, such as the growing economy, increasing urbanization, agricultural expansion and intensification, and various land use policies that have been launched in the past decade. In this section, we highlight the most significant dynamics exemplarily by means of subsets, as depicted in Figure 9.

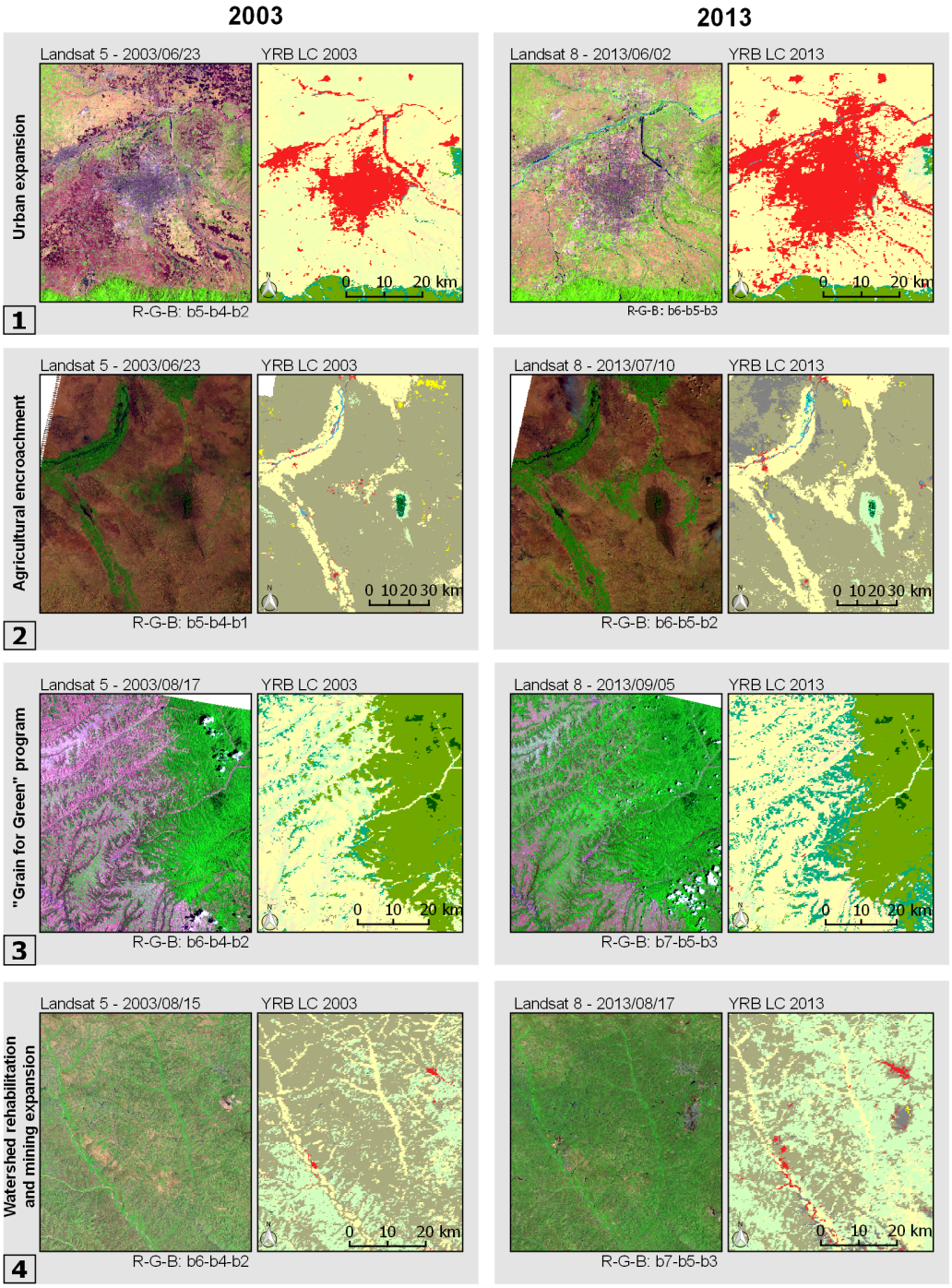

Figure 9. Local hotspots of change within the Yellow River Basin. The numbers refer to the exact geographical location as indicated in Figure 6. The color code of the different land cover types conforms to the colors introduced in Figure 6.

4.3.1. Urban Expansion

Despite population growth rates in China remaining more or less constant since 2003, the urbanization rate has almost doubled in this time [1]. This is also true for the Yellow River provinces, where urban areas of the major cities have expanded with an annual rate of up to 4%. Xi'an is the capital of Shaanxi province, which is one of the oldest cities in China, comprising a total present-day population of around 8.5 million, and growing annually by more than 3% (Figure 9 1). The city is embedded in the floodplains of the Wei River, a major region for agricultural production. As part of China's so-called "National Economic and Technological Development Zones", Xi'an is a center for high-tech industry and is specifically tailored to attract foreign investments and funds to foster local economies and employment. Artificial structures have further expanded mainly along river banks and in the major irrigation districts, where intense agricultural production is present. Throughout the basin, urban and built-up areas increased by almost 35% during the last decade.

4.3.2. Agricultural Encroachment

Agriculture is the dominant landscape feature in the Yellow River Basin, covering one third of the entire basin area. Between 2002 and 2013, the absolute numbers have not changed much, and there is even a noticeable decline in agricultural areas by 5%, which is in concordance with the national statistics [1] and can be seen in Table 4. Despite this overall decline, new areas for agricultural production have been developed locally in various regions. One example is located in the arid northern part of Ningxia province (Figure 9 2), where the establishment of new irrigation facilities has improved and intensified agricultural yields. Other examples of locally-encroaching agricultural fields are areas on the Ordos and Loess Plateau in Shaanxi province and Inner Mongolia, where the emergence of small-scale farming practices in groundwater-fed oases is presently located in the Ordos Desert. Another region experiencing significant agricultural dynamics and intensification is the Yellow River Delta region, mainly at the cost of the prevailing wetlands.

4.3.3. Ecological Restoration

Many decades and even centuries of intense human influence have turned particularly the Loess Plateau into a degraded landscape, where natural forests and shrublands in most areas were largely replaced centuries ago by agricultural cropland and pasture, contributing to recent severe soil erosion. In order to protect soils and maintain the fertility of such areas, diverse land use policies and conservation management plans have been launched to impede desertification, increase ecological conditions and sustain agricultural production, but in a more sustainable way. In the late 1990s, the Chinese government launched a nationwide scheme called the "Grain-for-Green" program, with the goal to increase and restore natural vegetation coverage on steep slopes of the Loess Plateau [64]. The change of the landscape structure as a result of this can be nicely seen in Figure 9, where grassland areas expanded on previous cropland or sparse land. The selected area is embedded in the Shanbei region (Shaanxi province).

In 1996, by the World Bank initiated the "Loess Plateau Watershed Rehabilitation Project" as one of the largest restoration programs worldwide and targeted specifically degraded areas with a low degree of vegetation coverage and susceptible to soil erosion. The primary objectives of this project were to create sustainable crop production on fertile arable land on terraced gulch slopes and to further stabilize land on slopes by planting a range of trees, shrubs and grasses to prevent soil degradation and erosion and the loss of valuable land to desertification. One target area is depicted in Figure 9, located in Gansu province, showing the successful recovery of grassland systems.

4.4. The YRB LC Product vs. Global and National Land Cover Products

Global land cover products are designed to delineate global land cover patterns, but their suitability for regional applications is not always given. We compare our regional land cover product

LC YRB 2013 to the MODIS MCD12Q1 2012 [19] (IGBP), the GlobCover 2009 [18] and the ESA CCI-LC 2010 [20]. Further, a high resolution Landsat 8 OLI scene (30 m) from 2013 was taken as reference imagery, showing finer prevailing landscape features in higher spatial detail. For this comparison, we have chosen three subregions, which characterize and represent the major landscape features in the Yellow River Basin determined by rather complex and heterogeneous conditions (Figure 10). The first subset (Row 1 in Figure 10) focuses on a semi-natural and agriculturally-dominated landscape with disjunct forest patches. The Yellow River Delta is the second subset, also a human-dominated landscape with biodiverse wetlands at the river mouth (second row). Further, we selected a rather natural ecosystem, the vast alpine grassland structures on the Qinghai-Tibet plateau presented in Column 3 of Figure 10. The geographical extent and distribution of each subregion is depicted in Figure 6.

The first region (Row 1 in Figure 10), located in the central part of Shaanxi province in the floodplains of the Wei River, covers disjunctive forest patches (deciduous and evergreen) surrounded by intensified agricultural areas. Transitional and fragmented areas of semi-natural vegetation are present at the forest edges, where small-scale farming practices cut the forest into small mosaics. Urban and peri-urban structures are scattered across the Wei floodplain, close to the capital of Shaanxi province (Xi'an). This complex landscape pattern is reflected in high spatial detail by the YRB LC 2013, which includes even the small-scale mosaic structure of natural and semi-natural vegetation patches. The continuous forest areas are delineated in all considered land cover maps. The MCD12Q1 tends to overestimate deciduous forest formations, and it fails to differentiate between forest types. Despite the lower class accuracies for open shrub- and wood-land and for the mosaic classes, their distribution is clearly discernible in the YRB LC 2013 map, considering this heterogeneous semi-natural landscape. Only ESA CCI-LC reflects the tessellated pattern in similar detail. Looking at the artificial class, our YRB LC 2013 map is exclusively able to delineate complex and small-scale urban structures.

In terms of complexity, a similar landscape is the Yellow River Delta, which is a region that has been intensively shaped by human interactions (Row 2 in Figure 10). The delta consists of very dynamic, temporally-flooded tidal flats and wetlands at the river mouth. Large aquaculture ponds intersect the near coastal zone and produce mainly fish and crustaceans [7]. The inner delta mainly consists of agricultural fields and many small scattered urban areas. Dongjing is the major city located in the southern delta region. Aquaculture ponds are depicted in the high resolution Landsat imagery and are congruent with the classified areas in YRB LC 2013. The other considered land cover maps clearly identified aquaculture incorrectly as either grassland, rainfed cropland or water bodies. While wetlands are often misclassified as grassland or irrigated cropland, cropland areas are depicted correctly in almost all land cover maps, except for ESA CCI-LC, where evident cropland areas are assigned to grassland. It can be further noted that urban areas seem to be better detected compared to the previous subset. GlobCover still greatly underestimates urban structures. Once again, YRB LC 2013 delineates these dispersed areas in higher spatial detail.

The third subregion, shown in Row 3 of Figure 10, covers rather homogeneous alpine grassland steppes (Qinghai province) interspersed with barren and sparse mountain ranges, showing low vegetation coverage. Two large freshwater lakes and small brackish water bodies are scattered across the area. Despite this homogeneity, the considered maps show different classification schemes, except for water bodies, which are delineated well in all maps. From the Landsat imagery, it is evident that YRB LC 2013 follows the landscape pattern of the high resolution image. The MODIS product classifies all terrestrial areas consistently as grassland and neglects sparse vegetation structures on mountainous areas. GlobCover captures barren structures, but assigns grassland steppes to mosaic croplands/vegetation and irrigated cropland classes. Furthermore, ESA CCI-LC introduces cropland-related classes in this area, even though agricultural production is not realistic in this harsh environment (altitude 4300 m) with its infertile soil and low temperatures.

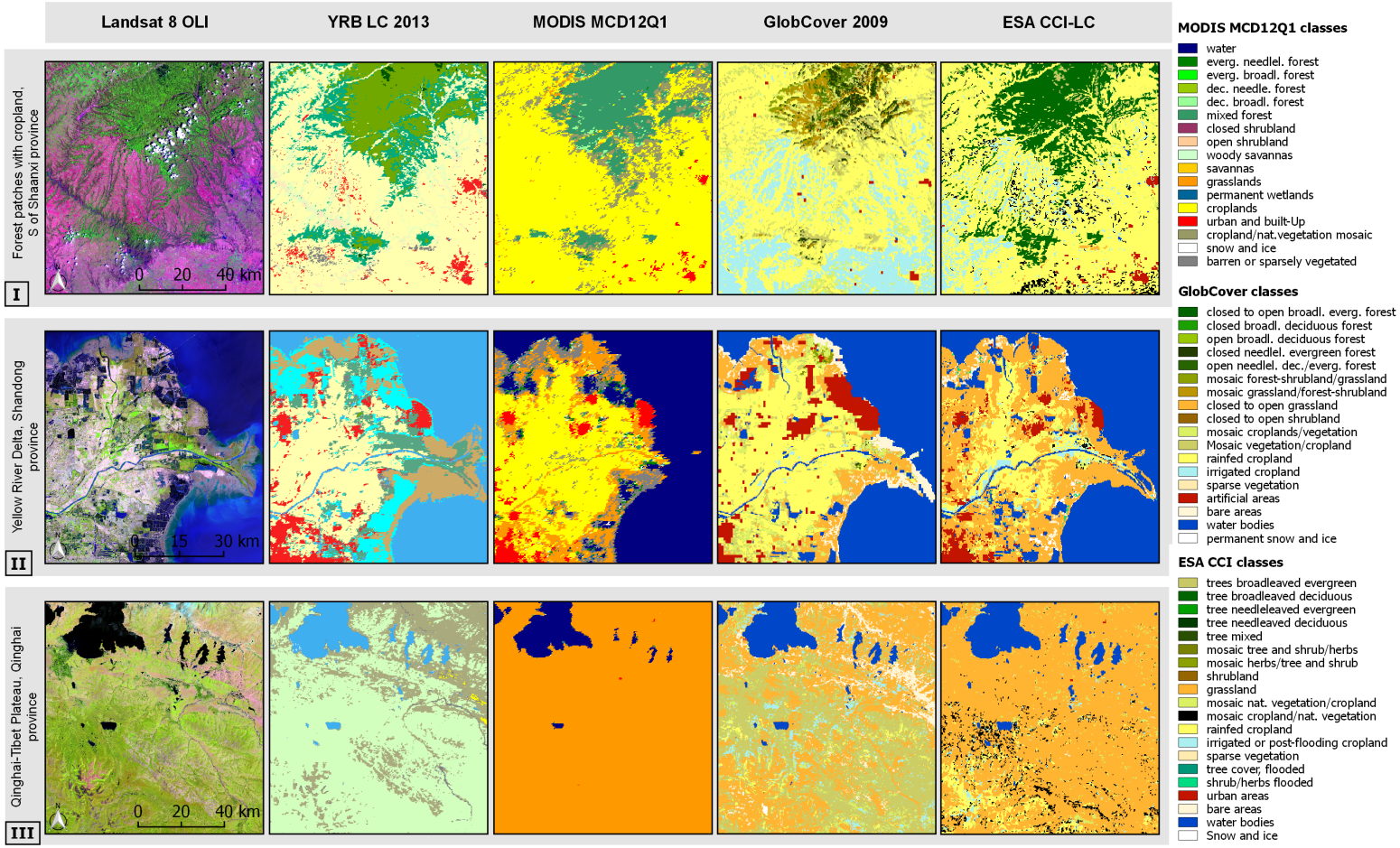

Figure 10. Comparison of Landsat 8 imagery (RGB band combination: 7-5-3; **Column 1**), against the YRB LC 2013 product (**Column 2**), MODIS MCD12Q1 2012 (**Column 3**), GlobCover 2009 (**Column 4**) and the ESA CCI-LC (**Column 5**) products. We selected three representative and rather heterogenetic subregions within the Yellow River Basin: a tessellated area with forest patches intersected with cropland in the south (Row 1); the delta area accompanied by urban, agriculture and wetlands (Row 2); and the source region dominated by grassland and sparse vegetation mosaics (Row 3). Color code for YRB LC 2013 as introduced in Figure 6.

5. Discussion

Prior work has highlighted the necessity of detailed, consistent and multi-temporal regional landscape information, making it important for climate or hydrological modeling, as well as for various decision-making processes. Hence, we developed in this paper novel land cover products for the very dynamic Yellow River Basin by revealing the current landscape characteristics and assessing past changes throughout the basin. A straightforward classification procedure was developed using high temporal moderate spatial resolution MODIS data, which enable accurate delineation of heterogeneous landscapes at large spatial scales.

5.1. Land Cover Classification and Dynamics

The two maps presented in this study describe the land cover status for the Yellow River Basin for the years 2003 and 2013. They provide thematic detailed and regionally-adapted land cover classes derived from high-temporal MODIS data at 250-m spatial resolution. For classification, we took spectral, phenological, temporal and ancillary information into consideration. In line with many studies using phenological information for land cover differentiation [24–26,29,65,66], we demonstrated the advantageous application of such data, particularly for regions comprising complex and heterogeneous environmental conditions. The Yellow River watershed covers an approximate area of 750,000 km^2 at an altitudinal gradient of more than 4600 m, therefore creating very diverse bioclimatic and environmental conditions.

The most obvious dynamics includes the landscape alteration of the Loess and Ordos Plateau, where land use policies and local conservation management plans combat the environmental deterioration by restoring vegetation cover and various ecosystem services, such as carbon sequestration, hydrological services and soil retention. As already shown in Sections 4.1 and 4.2, our results revealed changing ecological conditions, with the revegetation of barren and sparse land and transformation of sloped cropland to grass or woodland. Our results are analogous to a number of local remote sensing and landscape analysis studies, confirming an ecological and environmental enhancement also at larger scales [4,11,67–69]. Studies investigating the net primary productivity (NPP), a crucial proxy for vegetation productivity and carbon fluxes, indicated a steady increase over the last decade [70,71] stemming from land conservation programs. The study of Zhai *et al.*, 2015, emphasizes the strong anthropogenic effect on this landscape's changes and excluded precipitation as the driving factor, showing no significant correlation between precipitation and greening. Beside the emphasis on nature restoration, social facets also fall into the scope of the respective programs, aiming towards a reduction of the impoverishment of the local people.

Agriculture is a major landscape facet in the Yellow River Basin, and cultivation practices started centuries, even millennia ago. The Chinese government promotes the objective of food self-sufficiency in order to reduce the reliance on international trade markets [72]. Given the growing demand for food by a rising and increasingly affluent population, the agricultural sector is facing serious challenges to maintain food security, particularly considering progressive degradation of land and water resources. Absolute numbers of cultivated areas within the basin remained stable, while the total annual yield of agricultural commodities has tremendously increased [1] by means of improved farming practices, irrigation, fertilizer and pesticide consumption and more advanced machinery [73–76]. For instance, chemical fertilizer consumption has risen substantially by 10% in Shandon and even 32% in Henan province, the major production zones in the basin [1]. However, agricultural areas are still dynamic features across the basin, and we see certain localized changes. Declines in cultivated areas occurred mainly in Shaanxi, where the "Grain for Green" program took large areas out of cultivation [77]. With expanding and more efficient irrigation facilities, crop areas developed more strongly in arid regions, such as Northern Gansu or Ningxia, where the Yellow River and its tributaries provide a sufficient amount of water for irrigation. Multi-cropping harvest cycles per year are widespread in China to increase cropping intensity and yields without expanding the cultivated area. Located in the floodplains of the Wei River and North China Plain, these

multi-crop cycles mainly produce corn, wheat, oil-bearing crops, vegetables and fruits. Our results indicate a considerable decline of two seasonal cropping practices. Agricultural statistics from the National Bureau of Statistics reveal a decrease in total sown areas of winter wheat, replaced by more profitable crops, such as fruits or oil crops, which are showing an inverse trend [1]. However, the tremendous drop of two-season crops is not fully reflected in the statistics. There are various crop systems practiced in this region, periodically rotating from three-crop harvests in two years to annual harvests [78].

Urban and built-up areas have sprawled at tremendous speed, encroaching on surrounding lands covered by agriculture or natural vegetation. The economically most strongly developed provinces Shandong and Henan encompass the highest urban population exceeding 60% at annual growth rates up to 4%. Similar trends show less developed provinces, e.g., Qinghai or Ningxia, even at higher relative urbanization rates (10%). More and more peasants are moving to cities as those are the loci of employment and opportunities. Besides the urban sprawl of cities, built-up and artificial areas reveal significant encroachment along the river banks, where local industries and infrastructure emerged. Growing urbanization accompanied with a more affluent population usually leads to higher energy demands and consumption, mainly built on coal, which currently supplies two-thirds of China's overall energy use [1]. Coal production for domestic and international markets across the Yellow River Basin has increased by 25% in Shanxi province between 2003 and 2013, the major coal production center in the basin, and even by 300%, albeit from a low base [1]. This is reflected in our classified maps, where we can see localized emergence and expansion of mining areas and an increase of barren and impervious built-up land on the Ordos Plateau. Opencast mining activities have recently emerged and expanded in Qinghai province, replacing fragile and sensitive alpine grassland meadows.

5.2. Land Cover Accuracies

Given the very complex and heterogeneous landscape characteristics and the vast geographical extent, the attained thematic accuracies of 87% (2013) and 84% are satisfactory and comparable to other equally-complex regional land cover studies across the globe [24,26,29,45,65]. Seasonal information, based on high-temporal time-series data, is deemed to be a very important input feature in delineating different land cover classes, which can be seen in Figure 8. As illustrated in Table 3, the class-specific accuracies are in a high range, but classification challenges remain. Both mosaic classes and open deciduous broad-leaved shrub and woodland show the highest confusion, mainly with grassland, possessing user's accuracies of 65%–85% and producer's accuracies of 70%–86%. The error pattern is analogous for both years. According to our definition of the mosaic and open structure classes, the respective pixels may contain a significant area of grassland, making them quite similar in terms of spectral-temporal properties and, thus, leading to a false class allocation. Using medium-resolution remote sensing sensors, such as MODIS, and the accompanying lower accuracies, it was therefore necessary to introduce land cover mosaics to improve the thematic representation of the spatial heterogeneity inherent in the basin. Indeed, the major cause of misclassification is attributed to mixed pixels with the use of a conventional (hard) pixel classifier, particularly when the classification is based on medium to coarse resolution remote sensing data [58]. Similarity, open and closed forest systems, both evergreen and deciduous, often transit into each other and contribute to confusion between these classes. A fractional cover approach, where land cover proportions on a sub-pixel level are delineated, could lead to substantial enhancement of classification performance [25,79,80] for transitional and small-scale landscape structures, such as those occurring on the Loess Plateau.

Contrary to this, closed deciduous forests that occur in large-scale continuous patches have distinct spectral and temporal properties and were mapped with high accuracies exceeding 90%. Generally, spatially-homogeneous land cover types tend to have higher chances of being classified successfully. Analogically, the classes snow and ice, water bodies, tidal flats, wetlands and desert

yielded high class-specific accuracies with user's and producer's accuracies >90%, which usually encompass very distinct spectral and temporal signals and can be well mapped. Misclassification, albeit to a lower degree, appears in delineating aquacultural ponds with water bodies, barren land with deserts and barren areas with artificial and built-up surfaces. The latter case is an ambitious classification task, requiring the application of ancillary information. In this respect, we applied the Nighttime Lights Time Series for 2003 and 2013, which substantially helped to improve the final results.

6. Conclusions

This study presented a novel, consistent, thematically highly detailed and bi-temporal land cover analysis representing the heterogeneous land cover characteristics for the Yellow River Basin in China between 2003 and 2013 and revealing major changes in this dynamic region. Working at a spatial resolution of 250 m, we used the advances of phenology-based metrics derived from high-temporal MODIS time series to discern different land cover classes by their temporal trajectory at large spatial scales. Despite complex and challenging land surface characteristics, which include a wide range of land cover entities with different environmental conditions, the achieved thematic accuracies of 87% (2003) and 84% (2013) are promising. Although the tessellated land cover classes showed the lowest accuracies, the incorporation is necessary to give a better and more realistic representation of the spatial heterogeneity in the basin.

In conclusion, the presented classification scheme we presented, using spectral, seasonal and ancillary information, is a straightforward way to provide an enhanced picture of the prevailing landscape characteristics and dynamics on large spatial scales. To highlight the superiority of the regional-adapted maps, we compared the YRB LC product to the often used global land cover maps and clearly demonstrated that these optimized maps are better suited for depicting regional landscapes. Additionally, multi-temporal information allows for the spatial depiction of trends and recent land change across the Yellow River Basin. The major identified dynamics include agricultural and industrial intensification, as well as growing urban and peri-urban areas. Major conservation policies have considerably shaped the landscape characteristics and improved environmental and ecological conditions in the last decade. The developed highly detailed land cover maps provide essential information to support decision making for sustainable land and water management plans and are of particular interest for national, provincial and local stakeholders. Further, this information can be used as primary inputs for hydrological or climate modeling.

Acknowledgments: This study was undertaken in the context of the DELIGHT (Delta Information System for Geoenvironmental and Human Habitat Transition) project, funded by the German Federal Ministry of Education and Research, BMBF (Federal Ministry of Education and Research), and by the International Science and Technology Cooperation Program of China, 2012DFG22050. Furthermore, we would like to thank the MODIS and Landsat science team for providing the data free of charge. Finally, we would like to express our gratitude to Ursula Gessner for fruitful discussions and helpful insights that greatly helped to improve our manuscript. Three anonymous reviewers are thanked for greatly improving the quality of this contribution.

Author Contributions: Christian Wohlfart undertook the data precessing and analysis. Claudia Kuenzer and Gaohuan Liu designed the research scheme and guided the processing and interpretation. Christian Wohlfart authored the first version of the manuscript, and all authors jointly improved the version based on critical discussion. Chong Huang supported field work conducted in the Yellow River Basin.

Conflicts of Interest: The authors declare no conflict of interest.

References

1. NBS (National Bureau of Statistics) *China Statistical Database*; National Bureau of Statistics: Beijing, China, 2013.
2. Ringler, C.; Cai, X.; Wang, J.; Ahmed, A.; Xue, Y.; Xu, Z.; Yang, E.; Zhao, J.; Zhu, T.; Cheng, L.; *et al*. Yellow River basin: Living with scarcity. *Water Int.* **2010**, *35*, 681–701.
3. Nakayama, T. Simulation of the effect of irrigation on the hydrologic cycle in the highly cultivated Yellow River Basin. *Agric. For. Meteorol.* **2011**, *151*, 314–327.

4. Miao, C.Y.; Yang, L.; Chen, X.H.; Gao, Y. The vegetation cover dynamics (1982–2006) in different erosion regions of the Yellow River Basin, China. *Land Degrad. Dev.* **2012**, *23*, 62–71.
5. Cai, X. Water stress, water transfer and social equity in Northern China—Implications for policy reforms. *J. Environ. Manag.* **2008**, *87*, 14–25.
6. Bi, X.; Wang, B.; Lu, Q. Fragmentation effects of oil wells and roads on the Yellow River Delta, North China. *Ocean Coast. Manag.* **2011**, *54*, 256–264.
7. Ottinger, M.; Kuenzer, C.; Liu, G.; Wang, S.; Dech, S. Monitoring land cover dynamics in the Yellow River Delta from 1995 to 2010 based on Landsat 5 TM. *Appl. Geogr.* **2013**, *44*, 53–68.
8. Kuenzer, C.; Ottinger, M.; Liu, G.; Sun, B.; Baumhauer, R.; Dech, S. Earth observation-based coastal zone monitoring of the Yellow River Delta: Dynamics in China's second largest oil producing region over four decades. *Appl. Geogr.* **2014**, *55*, 92–107.
9. Dong, L.; Wang, W.; Ma, M.; Kong, J.; Veroustraete, F. The change of land cover and land use and its impact factors in upriver key regions of the Yellow River. *Int. J. Remote Sens.* **2009**, *30*, 1251–1265.
10. Song, X.; Yang, G.; Yan, C.; Duan, H.; Liu, G.; Zhu, Y. Driving forces behind land use and cover change in the Qinghai-Tibetan Plateau: a case study of the source region of the Yellow River, Qinghai Province, China. *Environ. Earth Sci.* **2009**, *59*, 793–801.
11. Chen, Y.F.; Liu, Y.S.; Wang, J.; Yan, J.P.; Guo, X.D. Land use changes of an aeolian-loessial soil area in Northwest China: implications for ecological restoration. *Pedosphere* **2009**, *19*, 356–361.
12. Guo, W.Q.; Yang, T.B.; Dai, J.G.; Shi, L.; Lu, Z.Y. Vegetation cover changes and their relationship to climate variation in the source region of the Yellow River, China, 1990–2000. *Int. J. Remote Sens.* **2008**, *29*, 2085–2103.
13. Liang, S.; Ge, S.; Wan, L.; Xu, D. Characteristics and causes of vegetation variation in the source regions of the Yellow River, China. *Int. J. Remote Sens.* **2012**, *33*, 1529–1542.
14. Zhang, X.; Sun, R.; Zhang, B.; Tong, Q. Land cover classification of the North China Plain using MODIS-EVI time series. *ISPRS J. Photogram. Remote Sens.* **2008**, *63*, 476–484.
15. Daofeng, L.; Chunhui, L.; Fanghua, H.; Zheng, L. Complex vegetation cover classification study of the Yellow River Basin based on NDVI data. In Proceedings of the 2004 IEEE International Geoscience and Remote Sensing Symposium, IGARSS '04, Anchorage, AK, USA, 20–24 September 2004; pp. 3360–3363.
16. Wang, S.; Ding, C.; Liu, J. Landscape evolution in the Yellow River Basin using satellite remote sensing and GIS during the past decade. *Int. J. Remote Sens.* **2009**, *30*, 5573–5591.
17. Bartholomé, E.; Belward, A.S. GLC2000: A new approach to global land cover mapping from Earth observation data. *Int. J. Remote Sens.* **2005**, *26*, 1959–1977.
18. Bicheron, P.; Defourny, P.; Brockmann, C.; Schouten, L.; Vancutsem, C.; Huc, M.; Bontemps, S.; Leroy, M.; Achard, F.; Herold, M.; Ranera, F.; Arino, O. *GLOBCOVER - Products Description and Validation Report*; MEDIAS-France: Toulouse, France, 2010.
19. Friedl, M.A.; Sulla-Menashe, D.; Tan, B.; Schneider, A.; Ramankutty, N.; Sibley, A.; Huang, X. MODIS Collection 5 global land cover: Algorithm refinements and characterization of new datasets. *Remote Sens. Environ.* **2010**, *114*, 168–182.
20. Defourney, P.; Kirches, G.; Brockmann, C.; Boettcher, M.; Peters, M.; Bontemps, S.; Lamarche, C.; Schlerf, M.; Santoro, M. *Land Cover CCI Product User Guide Version 2*; UCL-Geomatics: Louvain, Belgium, 2014.
21. McCallum, I.; Obersteiner, M.; Nilsson, S.; Shvidenko, A. A spatial comparison of four satellite derived 1 km global land cover datasets. *Int. J. Appl. Earth Obs. Geoinform.* **2006**, *8*, 246–255.
22. Herold, M.; Mayaux, P.; Woodcock, C.; Baccini, A.; Schmullius, C. Some challenges in global land cover mapping: An assessment of agreement and accuracy in existing 1 km datasets. *Remote Sens. Environ.* **2008**, *112*, 2538–2556.
23. Alcantara, C.; Kuemmerle, T.; Prishchepov, A.V.; Radeloff, V.C. Mapping abandoned agriculture with multi-temporal {MODIS} satellite data. *Remote Sens. Environ.* **2012**, *124*, 334–347.
24. Klein, I.; Gessner, U.; Kuenzer, C. Regional land cover mapping and change detection in Central Asia using MODIS time-series. *Appl. Geogr.* **2012**, *35*, 219–234.
25. Wohlfart, C.; Wegmann, M.; Leimgruber, P. Mapping threatened dry deciduous dipterocarp forest in South-east Asia for conservation management. *Trop. Conserv. Sci.* **2014**, *7*, 597–613.

26. Gessner, U.; Machwitz, M.; Esch, T.; Tillack, A.; Naeimi, V.; Kuenzer, C.; Dech, S. Multi-sensor mapping of West African land cover using MODIS, ASAR and TanDEM-X/TerraSAR-X data. *Remote Sens. Environ.* **2015**, *164*, 282–297.
27. Clark, M.L.; Aide, T.M.; Riner, G. Land change for all municipalities in Latin America and the Caribbean assessed from 250-m MODIS imagery (2001–2010). *Remote Sens. Environ.* **2012**, *126*, 84–103.
28. Kiptala, J.; Mohamed, Y.; Mul, M.; Cheema, M.; der Zaag, P.V. Land use and land cover classification using phenological variability from MODIS vegetation in the Upper Pangani River Basin, Eastern Africa. *Phys. Chem. Earth, Parts A/B/C* **2013**, *66*, 112–122.
29. Leinenkugel, P.; Kuenzer, C.; Oppelt, N.; Dech, S. Characterisation of land surface phenology and land cover based on moderate resolution satellite data in cloud prone areas—A novel product for the Mekong Basin. *Remote Sens. Environ.* **2013**, *136*, 180–198.
30. Hansen, M.C.; Townshend, J.R.G.; DeFries, R.S.; Carroll, M. Estimation of tree cover using MODIS data at global, continental and regional/local scales. *Int. J. Remote Sens.* **2005**, *26*, 4359–4380.
31. Hijmans, R.J.; Cameron, S.E.; Parra, J.L.; Jones, P.G.; Jarvis, A. Very high resolution interpolated climate surfaces for global land areas. *Int. J. Climatol.* **2005**, *25*, 1965–1978.
32. Miao, C.; Ni, J.; Borthwick, A.G.; Yang, L. A preliminary estimate of human and natural contributions to the changes in water discharge and sediment load in the Yellow River. *Glob. Planet. Chang.* **2011**, *76*, 196–205.
33. Chen, Y.; Syvitski, J.; Gao, S.; Overeem, I.; Kettner, A. Socio-economic impacts on flooding: A 4000-Year history of the Yellow River, China. *AMBIO* **2012**, *41*, 682–698.
34. Chen, L.; Wei, W.; Fu, B.; Lu, Y. Soil and water conservation on the Loess Plateau in China: Review and perspective. *Prog. Phys. Geogr.* **2007**, *31*, 389–403.
35. Olson, D.M.; Dinerstein, E.; Wikramanayake, E.D.; Burgess, N.D.; Powell, G.V.N.; Underwood, E.C.; D'amico, J.A.; Itoua, I.; Strand, H.E.; Morrison, J.C.; *et al.* Terrestrial ecoregions of the world: A new map of life on earth. *BioScience* **2001**, *51*, 933–938.
36. Wang, H.; Yang, Z.; Saito, Y.; Liu, J.P.; Sun, X.; Wang, Y. Stepwise decreases of the Huanghe (Yellow River) sediment load (1950–2005): Impacts of climate change and human activities. *Glob. Planet. Chang.* **2007**, *57*, 331–354.
37. Ran, L.; Lu, X.; Xin, Z.; Yang, X. Cumulative sediment trapping by reservoirs in large river basins: A case study of the Yellow River basin. *Glob. Planet. Chang.* **2013**, *100*, 308–319.
38. Huete, A.; Didan, K.; Miura, T.; Rodriguez, E.; Gao, X.; Ferreira, L. Overview of the radiometric and biophysical performance of the MODIS vegetation indices. *Remote Sens. Environ.* **2002**, *83*, 195–213.
39. R Core Team. *R: A Language and Environment for Statistical Computing*; R Foundation for Statistical Computing: Vienna, Austria, 2014.
40. Mattiuzzi, M.; Verbesselt, J.; Stevens, F.; Mosher, S.; Hengl, T.; Klisch, A.; Evans, B.; Lobo, A. *MODIS: MODIS Acquisition and Processing Package*. Available online: http://R-Forge.R-project.org/projects/modis/ (accessed on 10 February 2015).
41. Jönsson, P.; Eklundh, L. TIMESAT—A program for analyzing time-series of satellite sensor data. *Comput. Geosci.* **2004**, *30*, 833–845.
42. Savitzky, A.; Golay, M.J.E. Smoothing and differentiation of data by simplified least squares procedures. *Anal. Chem.* **1964**, *36*, 1627–1639.
43. Chang, J.; Hansen, M.C.; Pittman, K.; Carroll, M.; DiMiceli, C. Corn and soybean mapping in the United States using MODIS time-series data sets. *Agron. J.* **2007**, *99*, 1654–1664.
44. Conrad, C.; Colditz, R.R.; Dech, S.; Klein, D.; Vlek, P.L.G. Temporal segmentation of MODIS time series for improving crop classification in Central Asian irrigation systems. *Int. J. Remote Sens.* **2011**, *32*, 8763–8778.
45. Colditz, R.; Schmidt, M.; Conrad, C.; Hansen, M.; Dech, S. Land cover classification with coarse spatial resolution data to derive continuous and discrete maps for complex regions. *Remote Sens. Environ.* **2011**, *115*, 3264–3275.
46. Congalton, R.; Green, K. *Assessing the Accuracy of Remotely Sensed Data: Principles and Practices*; Mapping Science, CRC Press: Boca Raton, FL, USA, 2009.
47. Congalton, R.G. A comparison of sampling schemes used in generating error matrices for assessing the accuracy of maps generated from remotely sensed data. *Photogram. Eng. Remote Sens.* **1988**, *54*, 587–592.

48. Jensen, J.R. *Introductory Digital Image Processing: A Remote Sensing Perspective*; Prentice Hall: Upper Saddle River, NJ, USA, 2005.
49. Congalton, R.G. A review of assessing the accuracy of classifications of remotely sensed data. *Remote Sens. Environ.* **1991**, *37*, 35–46.
50. Chan, J.C.W.; Paelinckx, D. Evaluation of random forest and adaboost tree-based ensemble classification and spectral band selection for ecotope mapping using airborne hyperspectral imagery. *Remote Sens. Environ.* **2008**, *112*, 2999–3011.
51. Lawrence, R.L.; Wood, S.D.; Sheley, R.L. Mapping invasive plants using hyperspectral imagery and Breiman Cutler classifications (randomForest). *Remote Sens. Environ.* **2006**, *100*, 356–362.
52. Gislason, P.O.; Benediktsson, J.A.; Sveinsson, J.R. Random forests for land cover classification. *Pattern Recognit. Lett.* **2006**, *27*, 294–300.
53. Breiman, L. Random Forests. *Machine Learning*; Springer: New York, NY, USA, 2001; pp. 5–32.
54. Liaw, A.; Wiener, M. Classification and regression by randomForest. *R News* **2002**, *2*, 18–22.
55. Kuhn, M.; Wing, J.; Weston, S.; Williams, A.; Keefer, C.; Engelhardt, A.; Cooper, T.; Mayer, Z.; Kenkel, B.; the R Core Team, *et al*. *Caret: Classification and Regression Training*. Available online: http://CRAN.R-project. org/package=caret (accessed on 22 August 2015).
56. Kursa, M.B.; Rudnicki, W.R. Feature selection with the Boruta package. *J. Stat. Softw.* **2010**, *36*, 1–13.
57. Adelabu, S.; Mutanga, O.; Adam, E. Testing the reliability and stability of the internal accuracy assessment of random forest for classifying tree defoliation levels using different validation methods. *Geocarto Int.* **2015**, *30*, 810–821.
58. Foody, G. Status of land cover classification accuracy assessment. *Remote Sens. Environ.* **2002**, *80*, 185–201.
59. NOAA-NGDC. *Night-Time Lights of the World (Version 4)*. Available online: http://ngdc.noaa.gov/eog/dmsp/downloadV4composites.html (accessed on 22 August 2015).
60. Small, C.; Pozzi, F.; Elvidge, C. Spatial analysis of global urban extent from DMSP-OLS night lights. *Remote Sens. Environ.* **2005**, *96*, 277–291.
61. Li, L.; Friedl, M.A.; Xin, Q.; Gray, J.; Pan, Y.; Frolking, S. Mapping crop cycles in China using MODIS-EVI time series. *Remote Sens.* **2014**, *6*, 2473–2493.
62. Liu, J.; Wu, P.; Wang, Y.; Zhao, X.; Sun, S.; Cao, X. Impacts of changing cropping pattern on virtual water flows related to crops transfer: A case study for the Hetao irrigation district, China. *J. Sci. Food Agric.* **2014**, *94*, 2992–3000.
63. Guobin, L. Soil conservation and sustainable agriculture on the Loess Plateau: Challenges and prospects. *Ambio* **1999**, *28*, 663–668.
64. Zhou, H.; Rompaey, A.V.; Wang, J. Detecting the impact of the "Grain for Green" program on the mean annual vegetation cover in the Shaanxi province, China using SPOT-VGT NDVI data. *Land Use Policy* **2009**, *26*, 954–960.
65. Clark, M.L.; Aide, T.M.; Grau, H.R.; Riner, G. A scalable approach to mapping annual land cover at 250 m using MODIS time series data: A case study in the Dry Chaco ecoregion of South America. *Remote Sens. Environ.* **2010**, *114*, 2816–2832.
66. Blanco, P.D.; Colditz, R.R.; Saldaña, G.L.; Hardtke, L.A.; Llamas, R.M.; Mari, N.A.; Fischer, A.; Caride, C.; Aceñolaza, P.G.; del Valle, H.F.; *et al*. A land cover map of Latin America and the Caribbean in the framework of the SERENA project. *Remote Sens. Environ.* **2013**, *132*, 13–31.
67. Liu, J.; Li, Z.; Zhang, X.; Li, R.; Liu, X.; Zhang, H. Responses of vegetation cover to the Grain for Green Program and their driving forces in the He-Long region of the middle reaches of the Yellow River. *J. Arid Land* **2013**, *5*, 511–520.
68. Gao, P.; Niu, X.; Wang, B.; Zheng, Y. Land use changes and its driving forces in hilly ecological restoration area based on gis and rs of northern china. *Sci. Rep.* **2015**, *5*, 1–5.
69. Zhai, J.; Liu, R.; Liu, J.; Huang, L.; Qin, Y. Human-induced Landcover changes drive a diminution of land surface albedo in the Loess Plateau (China). *Remote Sens.* **2015**, *7*, 2926–2941.
70. Eisfelder, C.; Kuenzer, C. Investigating fourteen years of net primary productivity based on remote sensing data for China. In *Remote Sensing Time Series*; Springer International Publishing: Cham, Switzerland, 2015; pp. 269–288.
71. Feng, X.; Fu, B.; Lu, N.; Zeng, Y.; Wu, B. How ecological restoration alters ecosystem services: An analysis of carbon sequestration in China's Loess Plateau. *Sci. Rep.* **2013**, *3*, 1–5.

72. Ghose, B. Food security and food self-sufficiency in China: From past to 2050. *Food Energy Secur.* **2014**, *3*, 86–95.
73. Matson, P.A.; Parton, W.J.; Power, A.G.; Swift, M.J. Agricultural intensification and ecosystem properties. *Science* **1997**, *277*, 504–509.
74. Tilman, D.; Fargione, J.; Wolff, B.; D'Antonio, C.; Dobson, A.; Howarth, R.; Schindler, D.; Schlesinger, W.H.; Simberloff, D.; Swackhamer, D. Forecasting agriculturally driven global environmental change. *Science* **2001**, *292*, 281–284.
75. Rudel, T.K.; Schneider, L.; Uriarte, M.; Turner, B.L.; DeFries, R.; Lawrence, D.; Geoghegan, J.; Hecht, S.; Ickowitz, A.; Lambin, E.F.; *et al.* Agricultural intensification and changes in cultivated areas, 1970–2005. *Proc. Natl. Acad. Sci. USA* **2009**, *106*, 20675–20680.
76. Siebert, S.; Portmann, F.T.; Döll, P. Global patterns of cropland use intensity. *Remote Sens.* **2010**, *2*, 1625–1643.
77. Wang, J.; Liu, Y.; Liu, Z. Spatio-temporal patterns of cropland conversion in response to the "Grain for Green Project" in China's loess hilly region of Yanchuan County. *Remote Sens.* **2013**, *5*, 5642–5661.
78. Meng, E.C.; Hu, R.; Shi, X.; Zhang, S. *Maize in China: Production Systems, Constraints, and Research Priorities*; Maize Production Systems Papers 7648; (CIMMYT) International Maize and Wheat Improvement Center: El Batan, Mexico, 2006.
79. Fernandes, R.; Fraser, R.; Latifovic, R.; Cihlar, J.; Beaubien, J.; Du, Y. Approaches to fractional land cover and continuous field mapping: A comparative assessment over the BOREAS study region. *Remote Sens. Environ.* **2004**, *89*, 234–251.
80. Gessner, U.; Machwitz, M.; Conrad, C.; Dech, S. Estimating the fractional cover of growth forms and bare surface in savannas. A multi-resolution approach based on regression tree ensembles. *Remote Sens. Environ.* **2013**, *129*, 90–102.